LHCb 2007-144

LPHE 2008-001

Performance of the LHCb Track Reconstruction Software

M. Needham
Laboratoire de Physique des Hautes Energies,
École Polytechnique Fédérale de Lausanne

31st December 2007

Abstract

The performance of the LHCb track reconstruction software at the time of the DC 06 re-processing is described. For Long Tracks an event weighted efficiency of 91.4 % is found for a ghost rate of 14.6 %. For these tracks a momentum resolution of 4.2 per mille is obtained after a Kalman filter based fit.

1 Introduction

In this note the performance of the LHCb track reconstruction software at the time of the DC' 06 re-processing [1] is described. The LHCb tracking system (Fig 1) consists of a silicon vertex locator (VELO), a large area silicon station (Tracker Turicensis), magnet and three stations located downstream of the magnet. The latter, 'T' stations, are divided into an inner part (Inner Tracker) and an outer part (Outer Tracker). The detector covers the angular range 15 - 300 mrad which corresponds to $\eta = 2$ to 5.

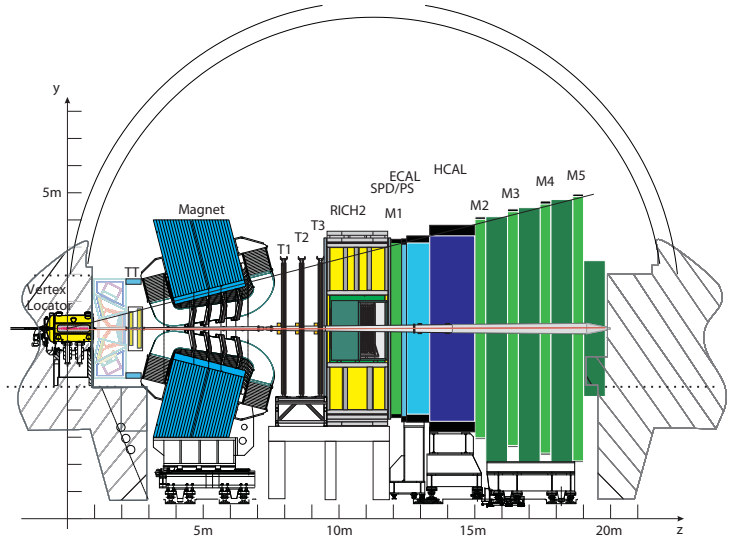

Figure 1: The LHCb detector (yz view).

The focus of this note is on the performance for tracks that traverse the entire spectrometer. These so called 'Long Tracks' are measured with the highest precision and are the most important sub-set for the reconstruction of B mesons. The reconstruction of Long Tracks proceeds as follows:

VELO Tracking: A stand-alone search is made for straight line track segments in the VELO [2]. For the DC '06 re-processing the performance of algorithm has been improved by the addition of a second pass algorithm based on linking spacepoints [3].

Forward Tracking: Continuations of the VELO tracks are searched for in the T stations using an optical method [4, 5].

Fit: The forward tracks are fitted using a Kalman filter algorithm which takes account of multiple scattering and energy loss within the detector [6, 7].

Seeding: A stand-alone search is made for track segments in the T stations [8]. Improvements to the performance of this algorithm for the DC '06 re-processing are summarized in [9].

Matching: The track segments found in the T stations are extrapolated upstream to the VELO. The track parameters are compared to those of the VELO track segments and a χ^2 criterion is used to select good matches [10]. Improvements to this algorithm for the DC '06 re-processing are summarized in [11].

Fit: The matched tracks are fitted using the Kalman filter.

Clone Killing: The tracks found by the forward tracking and matching are combined. As a final step a clone killing algorithm is run to select the best track from among those that share many hits [12]. If two or more tracks are flagged as clones the one with the most hits is selected. If the number of hits is equal the χ^2 is used to discriminate between competing candidates.

For both algorithms information from the TT station is added at the end of the pattern recognition step. In the case of the forward tracking it is one of several criteria used to validate the candidate track.

This note is organized as follows. First, changes to the simulation software between DC '04 and the DC '06 production are summarized. Next, the effect of the improvements to the pattern recognition since the start of DC '06 are quantified. The content in this part is similar to that in [13] and supersedes the results given there. This is followed by a discussion of the performance of the track fit for long tracks. For completeness the performance of the VELO tracking and T seeding are summarized in appendices together with the performance of the downstream tracking algorithm. The latter is tuned to find the products of hyperon decays occurring outside the VELO acceptance.

The performance studies were done using the following data samples:

- A sample of 12000 $\mathrm{B_d} \to J/\psi(\mu^+\mu^-)\mathrm{K_S}(\pi^+\pi^-)$ events generated at the default LHCb luminosity of 2×10^{32} cm^{-2}s^{-1}.
- A sample of 4000 $\mathrm{B_d} \to J/\psi(e^+e^-)K^*$ events generated at the default LHCb luminosity of 2×10^{32} cm^{-2}s^{-1}.

- Samples of 500 inclusive b events generated at luminosities of 5, 8, 10 and 20 $\times 10^{33}$ cm^{-2}s^{-1}.

The majority of results were obtained with the first sample. From the context it should be clear when this is not the case. The definitions of efficiency and ghost rate are given in Appendix D.

2 DC '06

Between DC '04 and DC '06 many changes were made to the LHCb simulation software in order to better reflect the constructed detector. The most significant changes are:

- A parameterization of the field map that more closely reflects measurements made in the pit is used.
- The detectors after the magnet (including the Inner and Outer Tracker) are now tilted by 3.2 mrad with respect to the beam-line.
- The material of the beam-pipe supports which previously was not described in the detector description has been added.
- New XML descriptions of the Tracker Turicensis and Inner Tracker have been implemented [14, 15]. These include detailed descriptions of inactive elements such as cables, cooling elements and frames.
- A more detailed digitization procedure for the Silicon Tracker has been implemented [16].
- The parameters in the digitization software of the VELO have been updated to agree with testbeam measurements. The resolution of VELO clusters is now more realistic but worse than that assumed at the time of DC '04.
- A more detailed digitization of the Outer Tracker has been implemented. The effect of after pulses is now included. In addition, the size of the Outer Tracker readout gate has been increased to 75 ns [17].

These changes mean the DC '06 simulation is significantly more realistic than that previously assumed. However, the environment for track reconstruction

is more challenging. The amount of material a track sees before RICH2 has increased from 40 to 50 % of a X_0 [18]. In addition, detector occupancies in the Inner and Outer Tracker have increased. This is mainly due to showering in the beam-pipe supports. The occupancy in the Inner Tracker has increased by 30 % [19] and the Outer Tracker occupancy by 40 % [20].

During this period the software framework has also evolved. The sub-detector and reconstruction event models were evaluated in a series of software reviews. For the tracking software this led to a new event that is described in detail in [21]. A track fitting procedure closely based on that used in the BaBar experiment has also been adopted. This procedure is robust against detector misalignments. Finally, the CLHEP package that was previously used for vector and matrix algebra has been replaced with a new package SMatrix.

3 Pattern Recognition performance

For long tracks an event weighted efficiency of 91.4 % is found [1]. This number is 2.0 % higher than the value found at the time of the DC '06 production [13]. In Fig. 2 the dependence of the efficiency on the pseudorapidity of the track is shown. Across most of the LHCb acceptance the efficiency is flat. However, there is a dip at a $\eta \sim 4.3$. This is attributed to the material of the 25 mrad section of the beam-pipe which lies within the acceptance of the detector. Fig. 3 shows the efficiency as a function of momentum. Below $\sim$ 10 GeV/c the efficiency falls rapidly. This is because the sizes of search windows are dominated by the effect of multiple scattering in the detector which increases at lower momenta. Above 10 GeV/c the efficiency plateaus at around 97 %.

The efficiency for reconstructing tracks that originate from B decays has also been investigated. The results are summarized in Table 1. For muons from $\mathrm{B_d} \to J/\psi(\mu^+\mu^-)\mathrm{K_S}(\pi^+\pi^-)$ a comparable performance to that obtained with the inclusive track sample is found. The performance for the electron case is worse reflecting the fact that bremsstrahlung in the material of the detector makes them harder to reconstruct. The efficiency for reconstructing pions from $\mathrm{B_d} \to J/\psi(\mu^+\mu^-)\mathrm{K_S}(\pi^+\pi^-)$ where the pion's give sufficient hits in the VELO to be reconstructible as long tracks is 88.5 %. This is 12 % higher than the corresponding DC' 06 number. Half of this improvement is attributed

[1] The corresponding track weighted number would be 90.6 %.

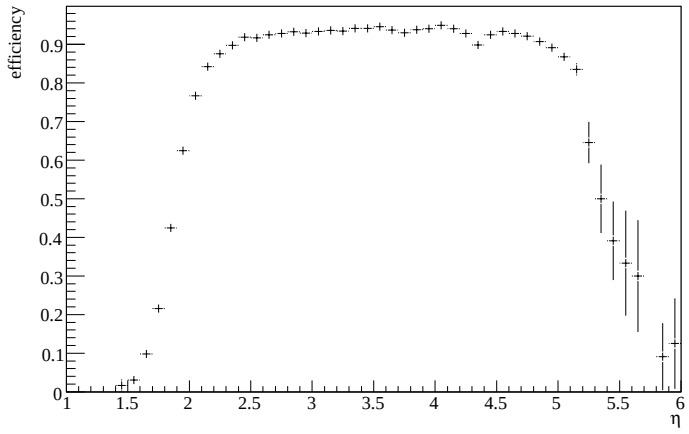

Figure 2: Track finding efficiency as a function of the pseudorapidity, η.

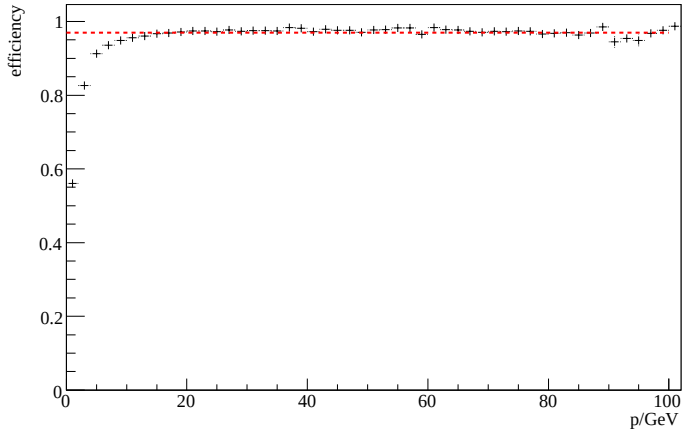

Figure 3: Track finding efficiency as a function of the momentum. The dashed line is at 97 % efficiency.

to the second pass VELO tracking algorithm that is tuned to find tracks of this type (see Appendix A). Another 2 % can be attributed to the general increase in the efficiency that has occurred since the DC '06 re-processing. This leaves an increase of 4 % in the efficiency unaccounted for [2].

[2]It is not ruled out that it is purely statistical, though it would have to be a 2 sigma effect.

Track type	$\overline{p}$/GeV	Efficiency (%)		
		Best	Forward	Match
$\mu^{\pm}$ from $B_d \to J/\psi(\mu^+\mu^-)K_S(\pi^+\pi^-)$	33	96.2	94.2	88.3
$e^{\pm}$ from $B_d \to J/\psi(e^+e^-)K_S(\pi^+\pi^-)$	34	92.0	86.7	84.7
$\pi^{\pm}$ from $B_d \to J/\psi(\mu^+\mu^-)K_S(\pi^+\pi^-)$	12	88.5	85.2	78.4

Table 1: Efficiencies for reconstructing tracks from specific B final states. Numbers are given for the combined long tracking (labeled Best) and also for the two long tracking algorithms.

Despite the running of the clone killing algorithm a clone rate of 2.2 % is observed. This is largely attributed to the VELO tracking algorithm which in some cases split the clusters coming from one particle into two tracks, one consisting of the hits from the forward stations and the other the hits of the remaining stations. Since the two tracks produced do not share hits they are not removed by the clone-killer. First studies show that an algorithm that compares track parameters [22] removes clones of this type with a negligible loss in efficiency. These studies will be documented in a future note.

The event weighted ghost rate is 14.6 % [3]. This number is 2.4 % lower than that found at the time of the DC' 06 production. In Fig. 4 the properties of ghost and real tracks are compared for four variables: the weighted number of measurements on the track defined as:

$$n_{meas} = n_{velo} + n_{TT} + n_{IT} + 0.5 \times n_{OT}\,[4],$$

the χ^2/ndof the track pseudorapidity and finally the track's transverse momentum. Compared to real tracks the ghosts have less measurements and have a worse χ^2/ndof. In addition, they tend to lie at high η and also around $\eta = 4.3$ [5]. Finally, it can be seen that ghost tracks have lower p_t than real tracks. By cutting either on one or a combination of these variables the ghost rate can be reduced at the cost of reduced efficiency. In addition, in the case of the Match tracks the criteria used to select a good combination of VELO and T-seeds is stored in the track and can be used to reduce the ghost rate [10]. For the forward tracks the quality variable used to rank and select tracks ('PatQuality') is stored. Studies to create a discriminating variable from a combination of these quantities are ongoing [23, 24].

[3] The corresponding track weighted number would be 19 %.

[4] The weight of 0.5 takes accounts of the fact that the OT gives twice the number of measurements per track to the IT.

[5] This effect is also attributed to the 25 mrad cone of the beam-pipe.

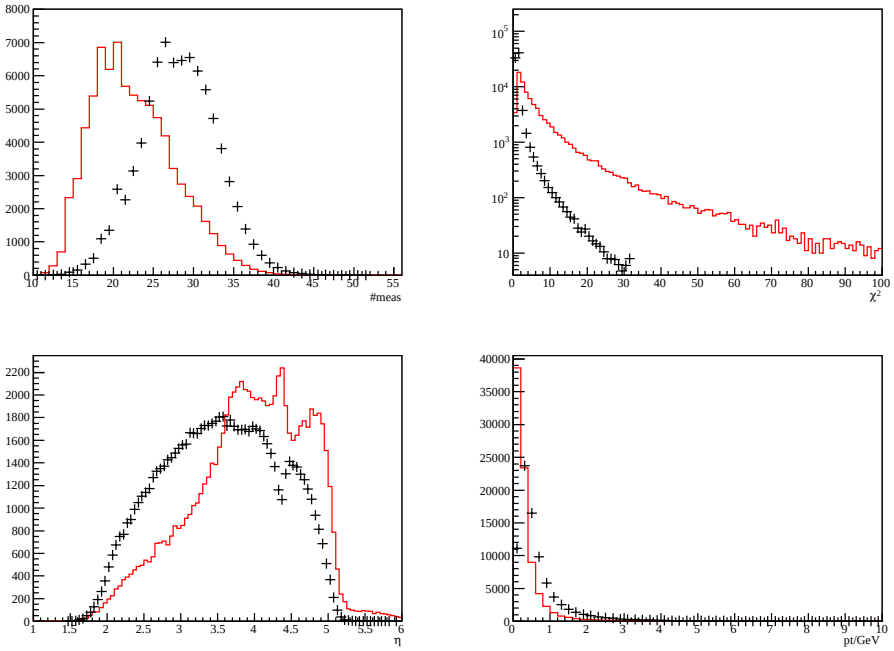

Figure 4: Comparison of the properties real (points) and ghost tracks (solid line). The four variables considered are: number of measurements (top left), χ^2/ndof (top right), η (bottom left), p_t (bottom right)

The simplest and most intuitive variable to use to reduce the ghost rate is the χ^2/ndof of the track fit. Fig. 5 shows the efficiency versus ghost rate as a function of a cut on this quantity. Such a cut also removes the majority of the ghosts with $\eta > 5.3$ which are outside the physical acceptance of the detector. This illustrates the fact that many of the variables that can be used to reduce the ghost rate are correlated.

3.1 Performance versus Luminosity

The performance as a function of the number of visible interactions as defined in [25] has been investigated. Fig. 6 shows the dependence of the efficiency and ghost rate on this quantity. It can be seen that the dependence of the efficiency on the number of visible interactions is weak. For each additional visible interaction in the detector the efficiency decreases by ~ 1 %. The ghost rate shows a clear dependence on the number of visible interactions

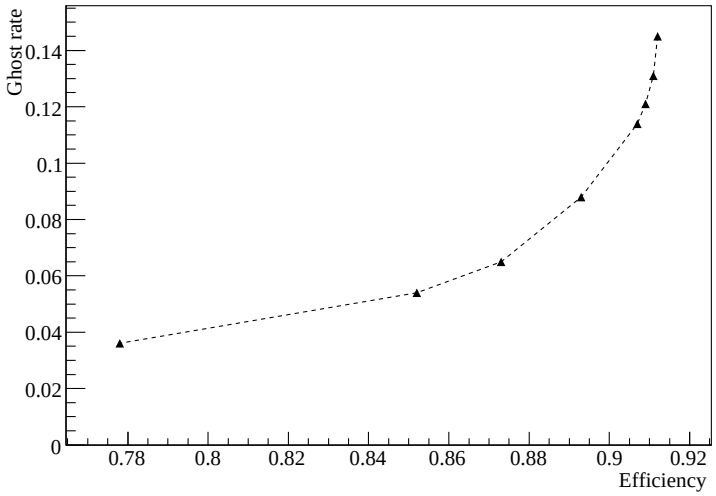

Figure 5: Efficiency versus ghost rate as a function of a cut on the χ^2/ndof. The points from left to right corresponds to cuts at 1.5, 2, 4, 6, 8, 10 ,15 and ∞.

in the detector. For each additional interaction the ghost rate increases by ~ 6 %. If only the number of visible interactions in the event spill influences the performance of the track reconstruction then efficiencies and ghost rates for an arbitrary luminosity can be derived directly from Fig. 6. Such a procedure is only valid if other effects, for example, the increased spillover at high luminosity can be neglected.

The performance of the long tracking up to luminosities of 2×10^{33} cm^{-2}s^{-1} has been also been studied directly. In the default version of the track seeding several cuts are applied to reject high multiplicity events and hot-spots in the detector in order to reduce the reconstruction time [9]. At very high luminosity these cuts will reject either a large fraction of events or sizable regions within events. Therefore, for these studies these cuts were removed. No further attempt was made to tune the reconstruction performance for the increased luminosity.

The results are summarized in Fig. 7. In this plot the efficiency and ghost rate as a function of luminosity are shown together with predictions made using Fig. 6. The latter are referred to as the limited spillover efficiency and ghost-rate. As can be seen the performance degrades linearly up to 1×10^{33} cm^{-2}s^{-1}. At high luminosities the efficiency starts to fall off more

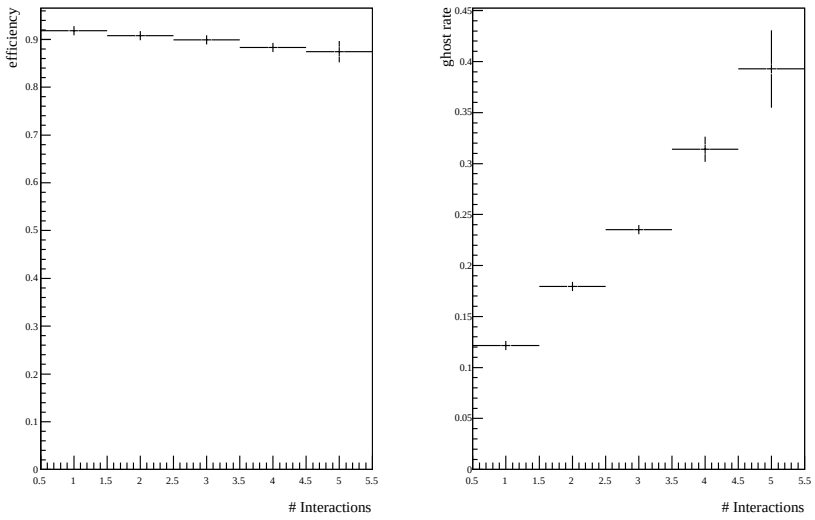

Figure 6: Efficiency (left) and ghost rate (right) versus the number of visible interactions.

rapidly. Above 5×10^{32} cm^{-2}s^{-1} the predicted values diverge from those found indicating that the effect of spillover becomes significant.

4 Track Fit Performance

The performance of the track fit at the start of the DC '06 production was not ideal. Since then detailed studies have led to improved performance. The changes made are as follows:

- Several bugs were found and fixed.
- The quality of the input tracks from the pattern recognition step has improved.
- Detailed studies have been carried out to tune the uncertainties on the cluster positions in the silicon detectors [26, 27].
- More attention has been paid to details in tolerances for extrapolations and also for the numerical evaluations of the closest distance of approach by the 'poca' tool [28].

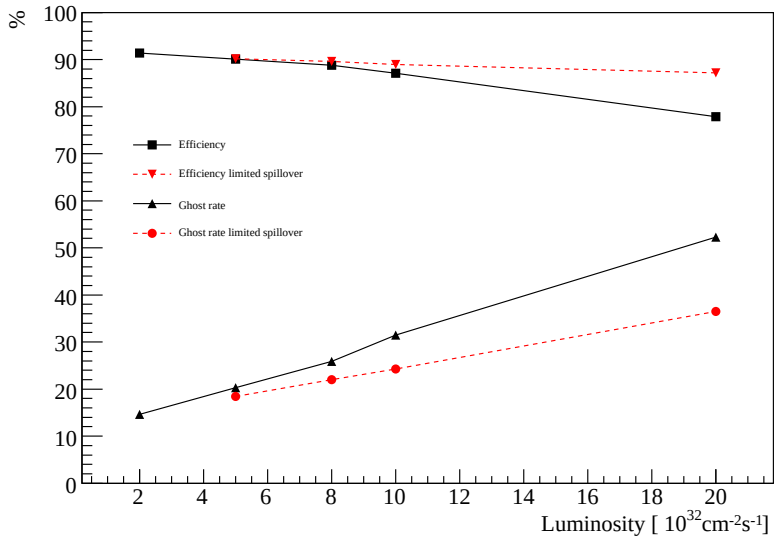

Figure 7: Long Tracking performance versus luminosity.

- The resolution of the L/R signs of the Outer Tracker measurements is now better handled [29].

The last of these is the most important change. Studies have indicated that mis-resolved L/R signs give rise to poorly reconstructed tracks and also slow the convergence of the fit necessitating many iterations [30]. To counter this a pre-fit is run. In this step the standard fit is run but the drift-time information from the Outer Tracker is ignored. After two iterations this procedure provides a reliable estimation of the L/R signs. Following this the fit is run including the drift-time information. Two iterations of the fit are performed followed by two iterations of outlier removal.

4.1 Fit Quality

In this section the quality of the track fit is discussed. In order to decouple possible effects from the pattern recognition step the results are compared to those obtained with so called ideal tracks. The latter are obtained using Monte Carlo truth to correctly assign hits to tracks and to provide an initial estimate of the track state.

One measure of the reliability of the fit are the pull distributions, namely the

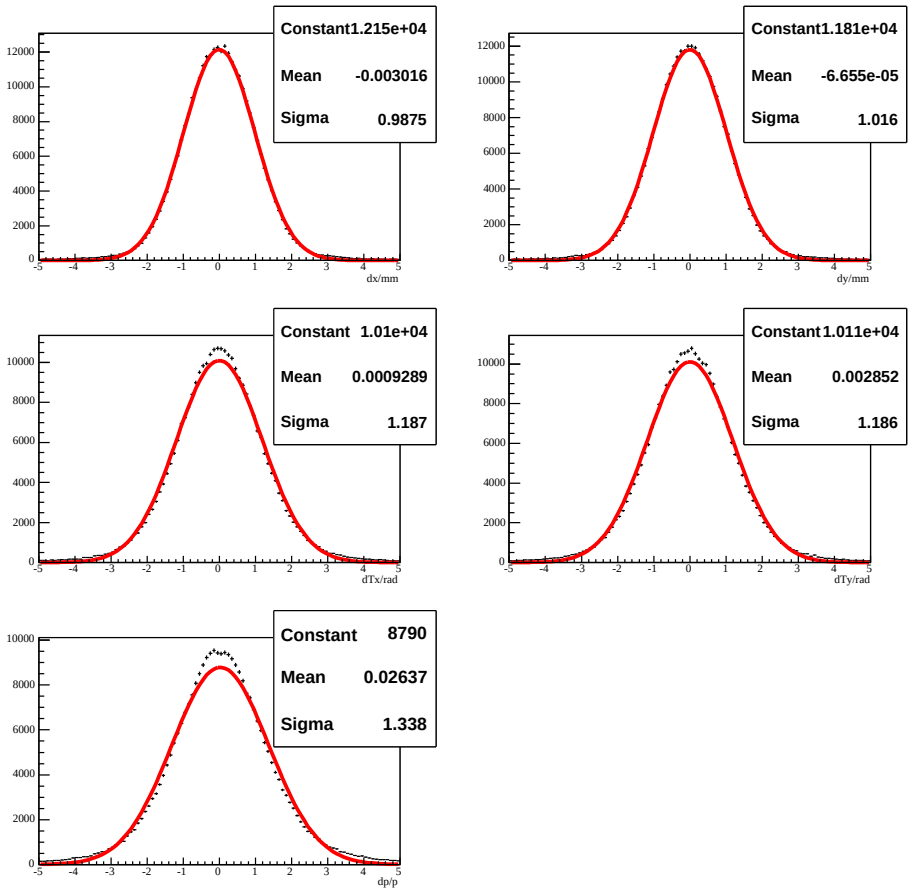

Figure 8: Pulls of the track parameters at the first measurement on tracks from the pattern recognition.

difference between the reconstructed and corresponding Monte Carlo quantity divided by the estimated uncertainty. If all the errors are Gaussian and properly taken into account each pull should follow a normal distribution centred on zero with unit variance. Fig. 8 shows the pulls at the first measurement on the track. It can be seen that all the pulls are centred on zero and well described by Gaussian fits. However, the sigma's of the pulls are generally larger than one. In Table 2 and 3 the sigma's of Gaussian fits to the pull distribution of the five track parameters (x, y, tx , ty, and q/p) are summarized for several locations along the track for both pattern recognition and ideal tracks. These show the same trend as at the first measurement: the pulls are generally larger than one indicating that the uncertainties on the track parameters are over-estimated. The effect is most pronounced for

the momentum parameter and also for the pulls at z = 216.5 cm (the exit of RICH1). The pulls are not unity due to several effects:

- Non Gaussian tails in the resolution function for the silicon detectors that are not accounted for in the assigned uncertainty [31]. In particular this explains the relatively poor pulls close to the location of the TT station.
- Mis-resolved L/R signs in the Outer Tracker.
- Differences in the multiple scattering and energy loss models assumed in the fit and those implemented in the version of Geant4 that was used to generate the Monte Carlo sample. First studies indicate that with a more recent version of Geant4, where the treatment of multiple scattering and energy loss is more reliable, the pulls on the momentum and track parameters are improved [32].

It can also been seen that there is no significant difference between the results obtained with ideal and pattern recognition tracks. As a further check the

Location	Pull				
	x	y	tx	ty	q/p
First Measurement	0.99	1.02	1.19	1.19	1.34
vertex	1.15	1.16	1.17	1.17	1.34
z = 80 cm	1.15	1.13	1.11	1.07	1.36
z = 216.5 cm	1.42	1.43	1.29	1.28	1.29
z = 750 cm	1.21	1.29	1.01	1.09	1.3
z = 945 cm	1.27	1.3	1.24	1.31	1.32

Table 2: Pulls at various positions on tracks from the pattern recognition.

sigma of the pulls of the slope parameters at the first measurement are plotted in Fig 9 as a function of the track momenta. No significant momentum dependence is observed.

A second measure of the fit quality is the probability of χ^2. If the model used in the fit accurately represents the particle trajectory this distribution should be flat. Fig. 10 shows the distribution of probability of χ^2 obtained for long tracks. The distribution is not flat — there is an accumulation around zero

Location	Pull				
	x	y	tx	ty	q/p
First Measurement	0.97	1.0	1.17	1.17	1.32
vertex	1.13	1.15	1.15	1.15	1.32
z = 80 cm	1.17	1.15	1.12	1.08	1.34
z = 216.5 cm	1.42	1.42	1.29	1.27	1.26
z = 750 cm	1.18	1.24	1.0	1.07	1.28
z = 945 cm	1.18	1.22	1.15	1.28	1.29

Table 3: Pulls at various positions on ideal tracks.

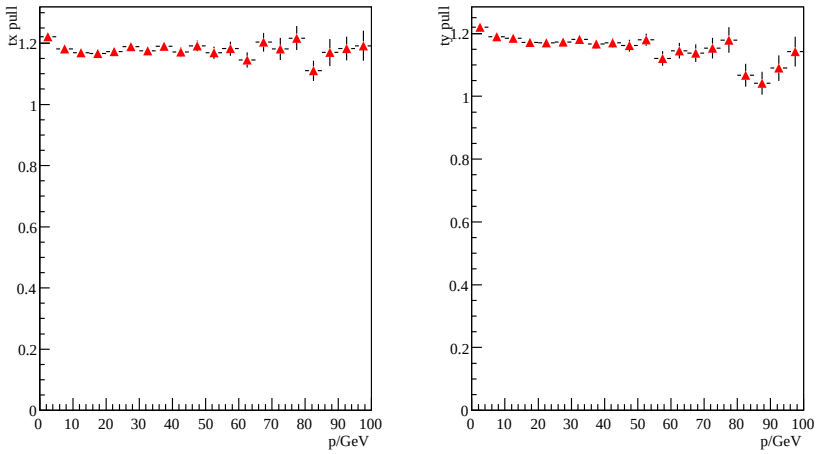

Figure 9: Pulls of the slope parameters, tx (left), ty (right) as a function of the track momentum at the z of the first measurement on the track.

probability that reflects the fact that the pulls are not unity. The distribution is reasonably well described by a β function :

$$\beta(p) = \frac{1}{Z(u_1, u_2)} p^{u_1 - 1}(1-p)^{u_2 - 1}$$

with $u_1 = 0.63$ and $u_2 = 0.86$.

Finally, as previously noted, the quality of the fit is strongly influenced by the fraction of correctly resolved L/R ambiguities in the Outer Tracker. Fig 11 shows the fraction of correctly resolved L/R ambiguities. This is defined as

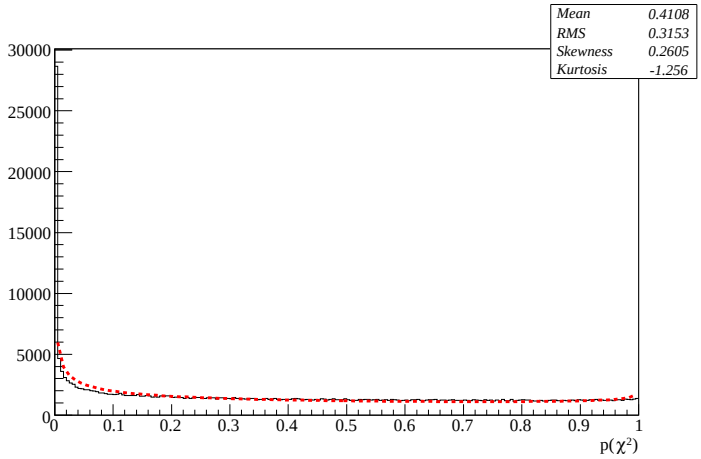

Figure 10: Probability of χ^2 for long tracks. The dotted line is the result of a fit to a β function.

the number of OT hits on a track with a correctly assigned L/R sign divided by the total number of OT hits. Close to the anode wire the L/R sign can not be reliably resolved. Therefore, only hits with a true drift distance of more than 300 μm are considered in the calculation. It can be seen that for 92 % of tracks all the L/R signs are correctly resolved.

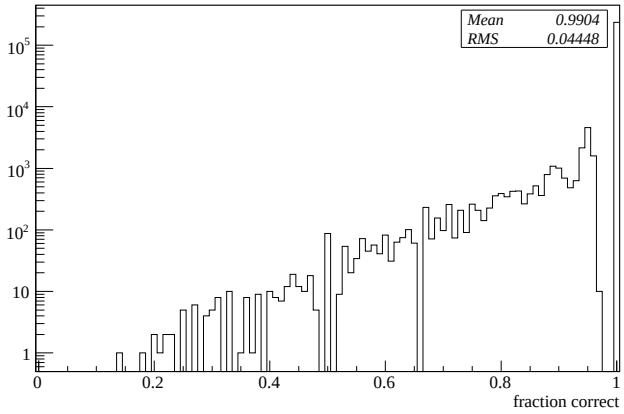

Figure 11: Fraction of correctly resolved L/R signs on a track.

The convergence of the fit has also been checked. Fig. 12 shows the momentum resolution and the mean probability of χ^2 as a function of the number of

fit iterations. It can be seen that after two iterations these quantities become stable indicating that the fit has converged.

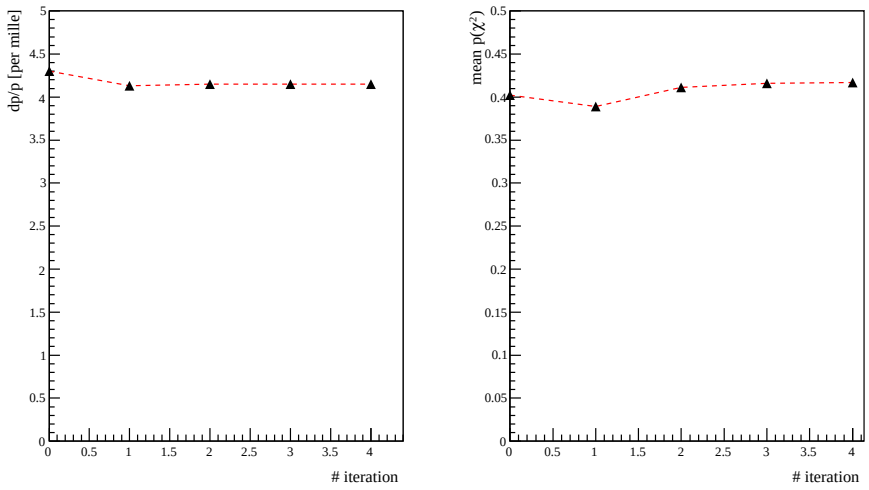

Figure 12: Momentum resolution (left) and mean p(χ^2) (right) as function of the number of fit iterations.

From these studies it is concluded that the fit procedure gives reliable estimate of the track parameters and covariance matrix.

4.2 Momentum Resolution Studies

The behaviour of the momentum resolution and pull as a function of the track momentum and pseudorapidity, η have been studied in detail. For tracks in the long acceptance a single Gaussian fit gives $\mathrm{dp/p} = 4.16 \times 10^{-3}$. Fig. 13 shows the momentum resolution and pull for pattern recognition and ideal tracks as a function of p whilst Fig. 14 shows the momentum resolution and pull as a function of η. Finally, Fig 15 shows the momentum resolution as a function of p for three bins in η. It can be seen that apart from at low momentum (and low η [6]) the fit of ideal and pattern tracks gives identical results. At low momentum the resolution for pattern recognition tracks is slightly worse than that of ideal tracks and consequently the pull

[6]Since low momentum tracks tend to be at low η these observations are equivalent.

over-estimated. Since this is the case it is expected that with further work the momentum resolution can be improved — though by a small amount.

As in the case of the pattern recognition the effect of the 25 mrad cone can clearly be seen. Tracks around $\eta = 4.3$ have a degraded momentum resolution and the pull is also overestimated. A degradation of the momentum resolution above $\eta = 4.5$ is also observed. This is due to two factors. First, the amount of material seen by a track increases at high η. This can be clearly seen in Fig. 16 where the amount material seen by a reconstructed track is plotted versus η. In addition, the angular coverage of the TT station extends only to $\eta \sim 4.6$. Previous studies [27] have shown that the information provided by the TT station is important for the determination of the momentum. This can be seen in Fig 17 where the momentum resolution of the standard track fit is compared to a run where the TT hits were excluded from the procedure. It can be seen that without TT information the momentum resolution degrades to 6 per mille.

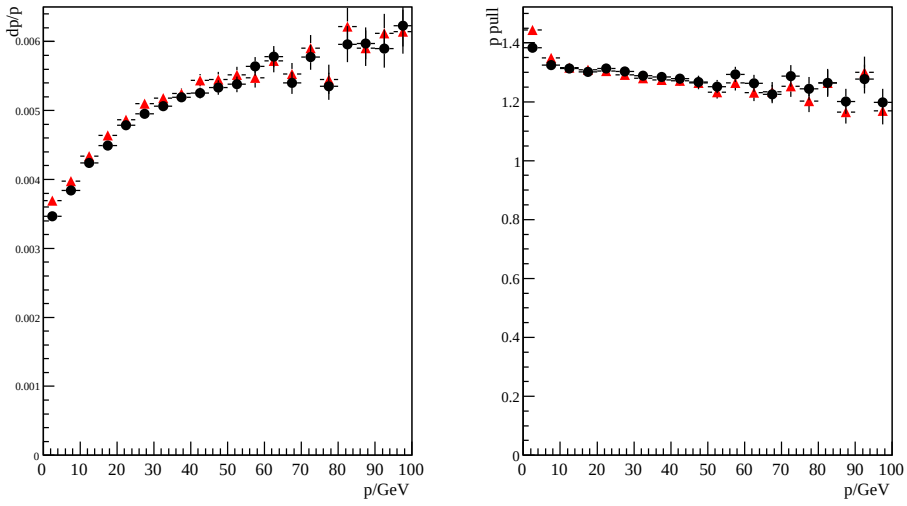

Figure 13: Momentum resolution (left) and momentum pull (right) as a function of p/GeV. The red triangles are the result of the fit of tracks from the pattern recognition whilst the black points are the result of the fit of the ideal tracks.

In Fig. 18 the dp/p obtained in these studies is compared to that found at the time of the DC '04 data challenge. At low momentum the resolution obtained is $\sim$ 10 % worse than that found in DC 04. This is consistent

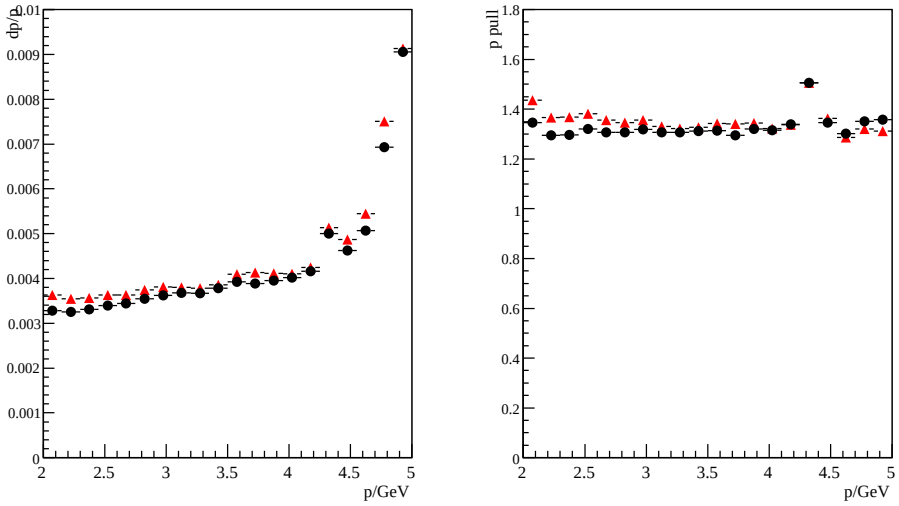

Figure 14: Momentum resolution (left) and momentum pull (right) as a function of η. The red triangles are the result of the fit of tracks from the pattern recognition whilst the black points are the result of the fit of the ideal tracks.

with the increase in the X_0 seen by a particle traversing the tracking system from 40 to 50 % of an X_0 that occurred between the two studies. At high momentum the degradation that has occurred is more pronounced and cannot be fully explained by the increase in detector material. The most likely cause is the worse resolution of the clusters in the silicon detectors.

For completeness, Fig. 19 shows the resolution on the track slopes at the first measurement. The observed behaviour is well described by the functional form:

$$\Delta t_{x,y} = \sqrt{A_{res}^2 + (B_{ms}/p[GeV])^2}$$

with $A_{res} = 6.2 \times 10^{-5}$ and $B_{ms} = 2.1 \times 10^{-3}$.

4.3 Fit Performance for electrons

The fit performance for electrons from $\mathrm{B_d} \to J/\psi(e^+e^-)\mathrm{K_S}(\pi^+\pi^-)$ has also been studied. Electrons undergo hard energy loss due to bremsstrahlung in the detector material. Typically a electron loses 30 % of its energy before z = 250 cm. Since the magnetic field in this region is low the direction

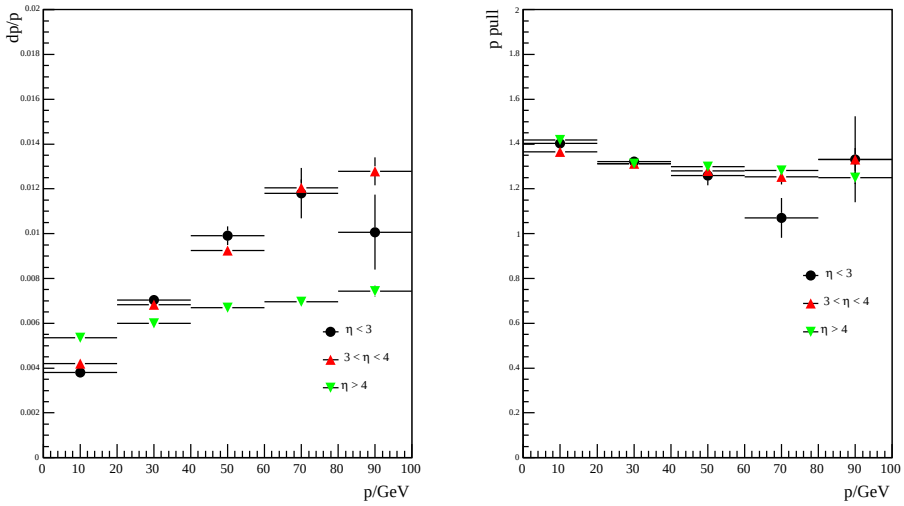

Figure 15: Momentum resolution (left) and momentum pull (right) as a function of p/GeV for three bins in η.

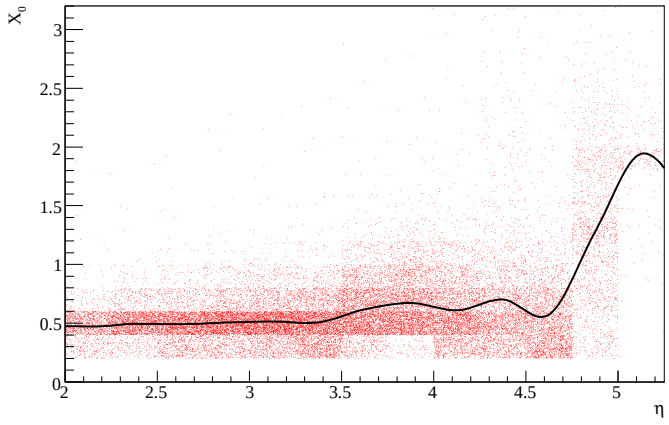

Figure 16: X_0 seen by reconstructed tracks as a function of η. The solid line is the average X_0 seen in each bin of η.

of the electron is practically unaltered by this process. Therefore, to first order, the momentum determined by the track fit is the value at the entrance (z $\approx$ 230 cm) or exit (z $\approx$ 750 cm) of the magnetic field. This is illustrated in Fig. 20 where the momentum resolution and pull for electrons

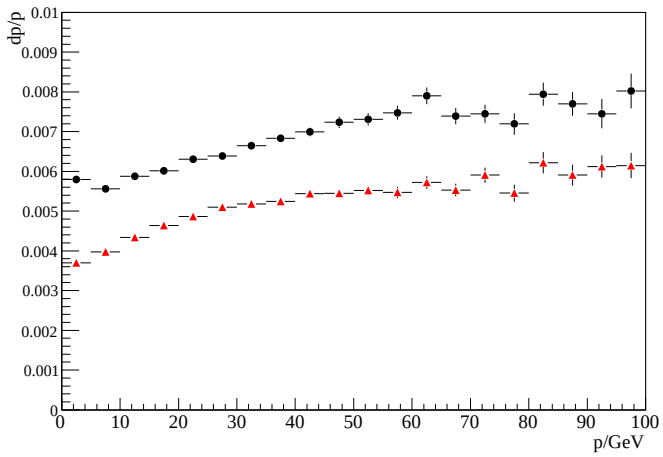

Figure 17: Momentum resolution as a function of p/GeV. The red triangles are in the case TT is used in the fit. The black points are if the TT hits are excluded from the fit.

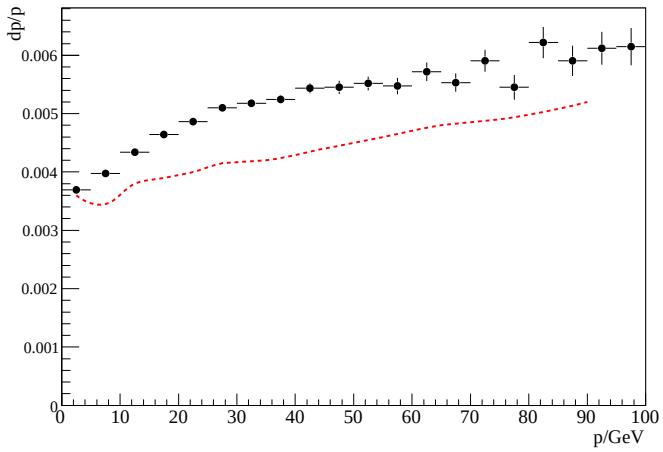

Figure 18: Momentum resolution, as a function of p/GeV, obtained in these studies (points) and DC 04 (dashed line). The DC 04 numbers are taken from [33].

from $B_d \rightarrow J/\psi(e^+e^-)K_S(\pi^+\pi^-)$ is plotted in one case using the true value of the track momentum at the production vertex and in the other using the true momentum at z = 750 cm. It can be seen that if the latter value is used

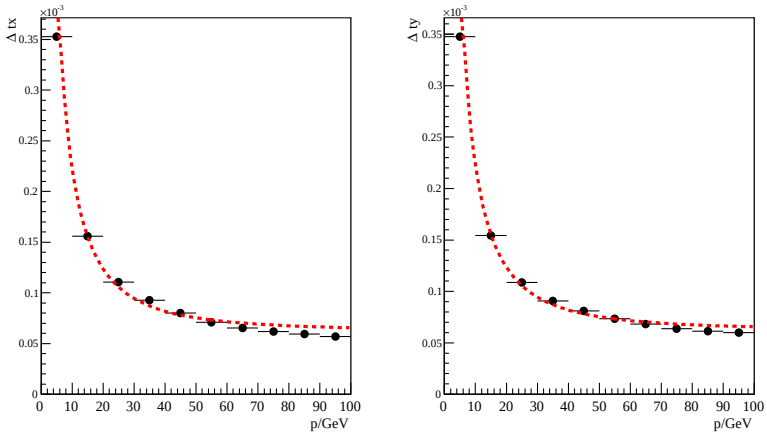

Figure 19: Resolution on tx (left) and ty (right) at the first measurement versus p/GeV. The dotted line is the functional form given in the text.

a core resolution of 5.1×10^3 is obtained. This is close to the momentum resolution for muons from $B_d \to J/\psi(\mu^+\mu^-)K_S(\pi^+\pi^-)$ of 4.5×10^{-3}. On the other hand if the true momentum of the electron at the vertex is used a long radiative tail is seen which is characteristic of bremsstrahlung in the detector material. The pull shows a similar behaviour. If the true momentum at z = 750 cm is used the momentum pull is 1.5 for the electron case to be compared with 1.3 in the muon case.

It is concluded that at the level of $\sim$ 10 % the fit for electrons correctly determines the momentum it is expected to measure, i.e. that at the entrance of the magnetic field. The error on this parameter is also well estimated. To determine the correct momentum at the vertex this information needs to be combined with information from the electromagnetic calorimeter [34, 35].

5 Summary

In this note the performance of the track fit at the time of the DC '06 reprocessing has been presented. An efficiency of 91.4 % has been achieved for a ghost rate of 14.6 %. This is similar to the performance found in previous studies [36, 37] and has been achieved despite the increased realism of the detector simulation. The performance of the reconstruction as a function of luminosity has also been studied. The performance of the detector degrades

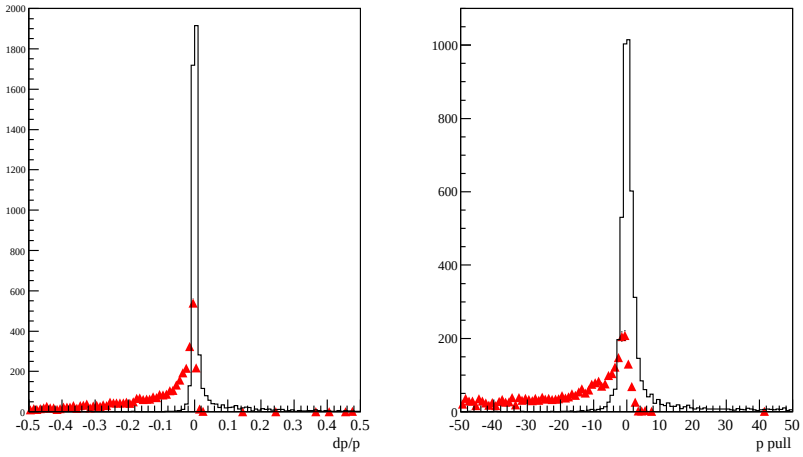

Figure 20: Momentum resolution(left) and momentum pull (right) for electrons from $B_d \to J/\psi(e^+e^-)K_S(\pi^+\pi^-)$. The solid line is obtained using the true momentum of the electron at z = 750 cm whereas the red points are obtained if the momentum of the electron at the first measurement on the track is used. *Nota Bene,* for the case of resolution (pull) at the first measurement 30 % (50 %) of the entries are in the underflow bin.

linearly up to a luminosity of 1×10^{33} cm^{-2}s^{-1}. This behaviour gives confidence that the reconstruction software is robust against further (unforeseen) increases in occupancy. Studies are ongoing to understand and reduce the ghost rate. If the ghost rate can be significantly reduced then it is possible that the efficiency can be improved.

A momentum resolution of 4.16×10^{-3} is found. This is 10 % worse than the value found at the time of DC '04. This degradation is mainly attributed to the increase in the material in the detector between DC 04 and DC 06. Though the performance of the fit is adequate some improvement is still possible since the momentum resolution of the ideal tracks is 4 per mille.

A VELO Tracking Performance

For the DC '06 re-processing a new strategy for VELO pattern recognition has been adopted. First, the algorithm described in [2] is run. This first searches for tracks in the r-z projection and then builds 3-D tracks by adding

the ϕ information. This is followed by a second pass algorithm (PatVeloGeneralTracking) which proceeds by building spacepoints from pairs of $r-\phi$ clusters in a station [3]. These are then linked together to form tracks. This second pass algorithm is tuned to find the decay products of hyperon decays occurring in the VELO far from the primary interaction region. The tracks from such decays are found with low efficiency by the first pass VELO algorithm since it makes cuts that require the track to be consistent with being produced in the primary interaction region.

The r-z tracking has an efficiency of 97.8 % for tracks within the long acceptance. The efficiency for tracks originating in the B decays is slightly higher (Table 4) apart from the decays products of hyperon decays where it is around 91 %. The ghost rate of the algorithm is 7.2 % and is dominated by tracks consisting of only three r hits [38].

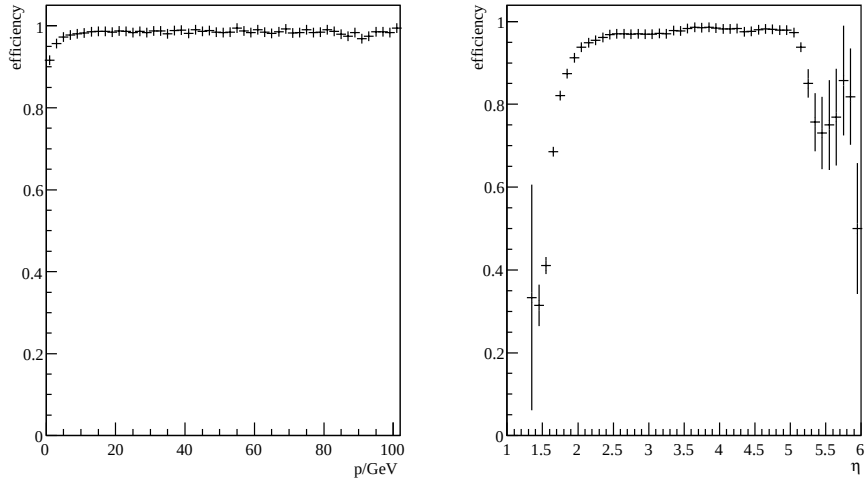

Figure 21: VELO tracking efficiency as a function of momentum (left) and as a function of η (right).

Next, the ϕ hits are added to create 3-D tracks. The efficiency of the combined 2-D and 3-D tracking procedure for tracks within the long acceptance is 95.3 % with a ghost rate of 4.5 %. After the second pass algorithm the efficiency is increases to 96.8 % for a ghost rate of 5.1 %. Table 5 summarizes the efficiency for reconstructing tracks from B final states whilst Fig. 21 shows the efficiency versus the track momentum and η. It should be noted that though the second pass algorithm is primarily aimed at increasing the

Track type	$\overline{p}$/GeV	Efficiency (%)
$\mu^{\pm}$ from $B_d \to J/\psi(\mu^+\mu^-)K_S(\pi^+\pi^-)$	33	98.9
$e^{\pm}$ from $B_d \to J/\psi(e^+e^-)K_S(\pi^+\pi^-)$	34	98.8
$\pi^{\pm}$ from $B_d \to J/\psi(\mu^+\mu^-)K_S(\pi^+\pi^-)$	12	91.1

Table 4: Efficiencies for reconstructing 2-D VELO tracks from specific B final states.

efficiency to find pions from K_s decays it also increases the efficiency to find other tracks. This translates into an increase in the long tracking efficiency. As can be seen from Table 6 there is a few per mille increase in the long tracking efficiency for tracks from other B final states.

Track type	$\overline{p}$/GeV	Efficiency (%)	
		Pass 1	Pass 1 + Pass 2
$\mu^{\pm}$ from $B_d \to J/\psi(\mu^+\mu^-)K_S(\pi^+\pi^-)$	33	96.8	98.4
$e^{\pm}$ from $B_d \to J/\psi(e^+e^-)K_S(\pi^+\pi^-)$	34	96.8	98.3
$\pi^{\pm}$ from $B_d \to J/\psi(\mu^+\mu^-)K_S(\pi^+\pi^-)$	12	84.5	92.9

Table 5: Efficiencies for reconstructing VELO tracks in the long acceptance from specific B final states.

Track type	$\overline{p}$/GeV	Efficiency (%)	
		Pass 1	Pass 1 + Pass 2
$\mu^{\pm}$ from $B_d \to J/\psi(\mu^+\mu^-)K_S(\pi^+\pi^-)$	33	95.8	96.2
$e^{\pm}$ from $B_d \to J/\psi(e^+e^-)K_S(\pi^+\pi^-)$	34	91.6	92.0
$\pi^{\pm}$ from $B_d \to J/\psi(\mu^+\mu^-)K_S(\pi^+\pi^-)$	12	82.3	88.5

Table 6: Efficiencies for reconstructing Long tracks from specific B final states with and without the second pass VELO tracking algorithm.

B T-seeding Performance

The T-seeding algorithm is described in detail in [8, 9] and [39]. For tracks within the long acceptance an efficiency of 92.7 % is found for a ghost rate of 7.2 %. Fig. 22 shows the efficiency as a function of momentum. It can be seen that above $\sim$ 5 GeV/c the efficiency of the algorithm is 97 %. Efficiencies for track from B final states are summarized in Table 7.

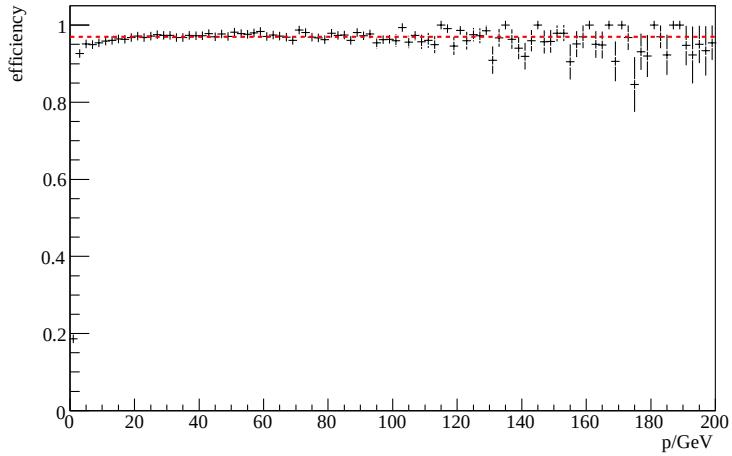

Figure 22: T-seeding efficiency as a function of momentum. The dashed line is at 97 % efficiency.

Track type	$\overline{p}$/GeV	Efficiency (%)
$\mu^{\pm}$ from $B_d \to J/\psi(\mu^+\mu^-)K_S(\pi^+\pi^-)$	33	96.3
$e^{\pm}$ from $B_d \to J/\psi(e^+e^-)K_S(\pi^+\pi^-)$	34	93.8
$\pi^{\pm}$ from $B_d \to J/\psi(\mu^+\mu^-)K_S(\pi^+\pi^-)$(VELO)	12	93.5
$\pi^{\pm}$ from $B_d \to J/\psi(\mu^+\mu^-)K_S(\pi^+\pi^-)$(Downstream)	36	93.8

Table 7: Efficiencies for reconstructing T-seeds for tracks from B final states.

C Downstream Tracking Performance

The downstream tracking algorithm is described in [40]. It is tuned to find the products of hyperon decays occurring outside the VELO acceptance. The efficiency of the algorithm for tracks in the downstream acceptance is 74.2 % for a ghost rate of 27.2 %. For pions from $B_d \to J/\psi(\mu^+\mu^-)K_S(\pi^+\pi^-)$ in the downstream acceptance the efficiency is higher around 82.3 %. The efficiency as a function of momentum and η is shown in Fig. 23. The efficiency of the algorithm drops at both high momentum and high η. The latter effect reflects the fact that the angular coverage (and hence the number of hits it gives) of the TT station above $\eta \sim 4.6$ is limited. Since high momentum tracks tend to be at high η this may also explain the drop in the efficiency of the algorithm at high momentum. Further studies are needed to verify if this is the case or whether other factors, such as search windows being too tight, cause the observed loss in efficiency.

There is also a dip in the efficiency around $\eta = 3.7$ [7]. This value of η roughly corresponds to the location of the PCB and connectors for the Inner Tracker signal cables [15]. Therefore, a possible explanation is that multiple scattering in this material causes the efficiency loss. On other hand it could be caused by an inefficiency in the seeding algorithm for tracks passing through the overlap region between the Inner and Outer Tracker. Again further studies are needed to confirm which hypothesis is correct.

The momentum resolution and pull for long tracks are shown in Fig. 24. At low momentum the resolution obtained is as good as that found for long tracks. This reflects the observation, alluded to in Section 4.2, that at low momentum the resolution of the detector is determined by the T stations and TT alone. Only at high momentum does the VELO significantly improve the momentum resolution.

D Definitions

To produce the plots an extended version of the **TrackCheckers** package was used. This contains two algorithms **TrackEffChecker** and **TrackResChecker** that allow the performance of the pattern recognition and fit to be checked. The majority of the plots contained in this note are produced by default by these algorithms. Both algorithms derive from a common base

[7] Close examination of Fig. 2 shows a similar drop around $\eta = 3.7$ for long tracks.

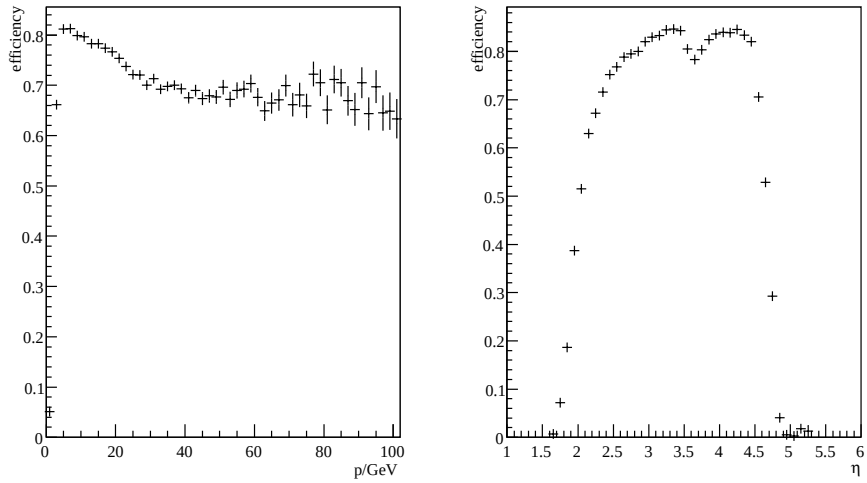

Figure 23: Downstream tracking efficiency as a function of momentum (left) and as a function of η (right).

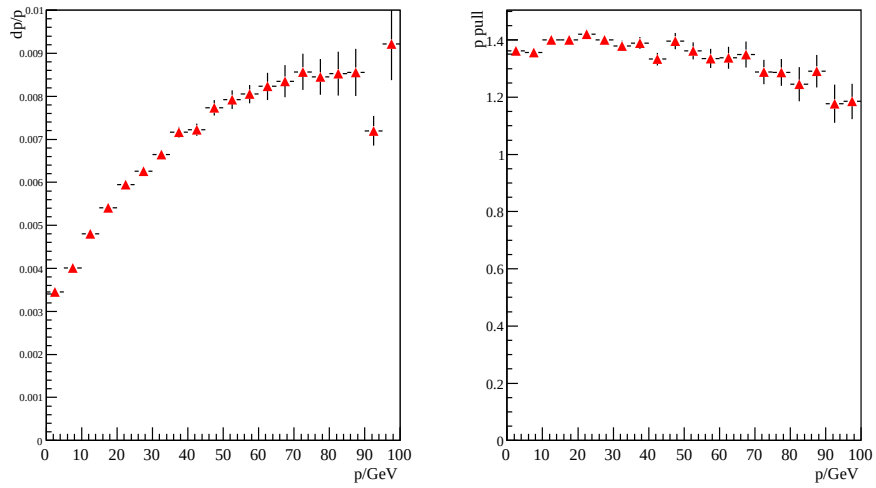

Figure 24: Momentum resolution (left) and momentum pull (right) as a function of p/GeV for Downstream tracks.

class **TrackCheckerBase** which provides access to standard tools and functions.

To define the set of reconstructible tracks these algorithms make use of the **MCReconstructible** tool. This implements the standard definitions of long and downstream tracks. A particle is defined to be in the long acceptance if it satisfies the following criteria:

- The particle momentum at its production vertex is more than 1 GeV/c.
- Three reconstructed clusters in the r sensors of the VELO.
- Three reconstructed clusters in the ϕ detectors of the VELO.
- A reconstructed x and u hit in each of the tracking stations T1-T3.
- It does not interact hadronically before the end of the T stations.

The definition of the downstream acceptance is the same apart from the fact that the requirements on the number of VELO clusters are removed and replaced by the requirement that the track should give at least one hit in TTa and TTb.

The track reconstruction efficiency is given by:

$$\text{efficiency} = \text{N(accepted } \cap \text{ track reconstructed)/N(accepted)}$$

For the efficiency calculation all particles except electrons satisfying the above acceptance criteria are used regardless of their origin. Electrons are excluded because the majority originate in secondary interactions such as photon conversions. These have little physics interest but are more difficult to reconstruct due to subsequent bremsstrahlung in the detector material. To determine whether a Monte Carlo has been reconstructed an association algorithm is needed. A track is said to be related to a true particle (**MCParticle**) if more than 70 % of the clusters in the VELO come from that particle and more than 70 % of the hits in the seeding region also come from that particle. The other important indicator of the tracking performance is the ghost rate. The is defined as:

$$\text{ghost rate} = \text{N(rec tracks not related to a } \mathbf{MCParticle}\text{)/N(rec tracks)}$$

Both the efficiency and the ghost rate can be calculated in two ways. The first is to calculate these quantities on an event-by-event basis ('event weighted'). If values for the whole event sample are required the averages of the resulting distributions are used. The alternative is simply to calculate the efficiency and ghost rate on the whole sample of tracks ignoring which event the track came from ('track weighted').

References

[1] Gauss v25r7, Boole v12r10, Brunel v31r11, XmlDDDB v30r14.

[2] D. Hutchcroft *et al.* VELO Pattern Recognition. LHCb-note 2007-013.

[3] D. Hutchcroft, New tracking algorithm to catch Velo Ks tracks after 3D pattern recognition, T-Rec meeting, 2^{nd} July 2007.

[4] M. Benayoun and O. Callot. The forward tracking, an optical model method. LHCb-note 2002-008.

[5] O. Callot and S. Menzemer. Performance of the forward tracking. LHCb-note 2007-015.

[6] M. Merk *et al.* Performance of the LHCb OO Track Fitting Software. LHCb-note 2006-086.

[7] E. Rodrigues. The LHCb Kalman Fit. LHCb-note 2007-014.

[8] R. Forty M. Needham. Standalone Track Reconstruction in the T-Stations. LHCb-note 2007-022.

[9] R. Forty and M. Needham. Updated Performance of the T seeding. LHCb-note 2007-023.

[10] J. van Tilburg and M. Needham. Performance of the Track Matching. LHCb-note 2007-020.

[11] M. Needham. Performance of the Track Matching. LHCb-note 2007-129.

[12] E. Rodrigues. Dealing with clones in the Tracking. LHCb-note 2006-065.

[13] M. Needham. Combined Long Tracking Performance. LHCb-Note 2007-019.

[14] M. Needham D. Volyanskyy. Updated geometry description for the LHCb Trigger Tracker. LHCb-note 2006-032.

[15] A. Perrin and K. Vervink. The Inner Tracker detector description and its implmentation in the XML database. LHCb-note 2006-018.

[16] M. Needham, Tracking System Performance for DC 06 , LHCb-Software Week, 26^{th} April 2006.

[17] J. Nardulli. Outer Tracker Occupancy Studies. LHCb-Note 2005-092.

[18] M. Needham and T. Ruf. Estimation of the material in the LHCb detector. LHCb-note 2007-025.

[19] M. Needham. ST Occupancies and Clustering. LHCb-note 2007-024.

[20] J. Amoraal. OT simulation. LHCb-note 2007-018.

[21] J. Hernando Morata and E. Rodrigues. Tracking event model. LHCb-note 2007-007.

[22] M. Needham, Clones: A New Approach, T-Rec meeting, 13^{th} August 2007.

[23] A. Perieanu, Finding Ghost Tracks with Neural Nets, Tracking and Alignment Workshop, Amsterdam, 31^{st} August 2007.

[24] M. Needham, , Tracking and Alignment Workshop, Amsterdam, 31^{st} August 2007.

[25] The LHCb Collaboration. Reoptimized Detector Design and Performance. CERN/LHCC LHCC-2003-030.

[26] T. Szumlak C. Parkes and T. Ruf. Reconstruction of Cluster Positions in the LHCb VELO. LHCb-note 2007-151.

[27] M. Needham, Tracking News, T-Rec meeting, 2^{nd} July 2007.

[28] E. Bos *et al.* The Trajectory Model for Track Fitting and Alignment. LHCb-Note 2007-008.

[29] M. Needham, Tracking Status for DC 06, LHCb-Software Week, CERN, 4^{th} October 2007.

[30] M. Needham, T-Rec Meeting, Momentum Resolution Studies, 11^{th} June 2007.

[31] W. Hulsbergen, Tracking and Alignment Workshop, Heidelberg, 22^{nd} February 2007.

[32] E. Bos, Tracking and Alignment Workshop, Amsterdam, 31^{st} August 2007.

[33] J. van Tilburg. *Track Simulation and Reconstruction in LHCb.* PhD thesis, Vrije Universitett, 2005.

[34] M. Needham. Electron Reconstruction Studies. LHCb-Note 2001-102.

[35] H. Terrier. *Étude de la violation de CP dans le canal $B_d^0 \to J/\phi(ee)K_s^0$, identification et reconstruction des électrons dans l'éxperience LHCb.* PhD thesis, Uni. de Savoie, 2005.

[36] M. Needham. Status and Expected Performance of the LHCb Tracking System. *Nuclear Physics B*, (156):217–220, 2006.

[37] M. Needham. Tracking Performance and Robustness Tests. LHCb-note 2003-020.

[38] M. Needham. Classification of Ghost Tracks. LHCb-note 2007-129.

[39] M. Needham. The Tsa Reconstruction Framework. LHCb-Note 2007-037.

[40] O. Callot. Downstream Pattern Recognition. LHCb-Note 2007-026.